The 2nd IBIS/ISGRI soft gamma-ray survey catalog[1]

A. J. Bird[a], E. J. Barlow[a], L. Bassani[b], A. Bazzano[c], G. Bélanger[d,e], A. Bodaghee[f] F. Capitanio[a,c], A. J. Dean[a], M. Fiocchi[c], A. B. Hill[a], F. Lebrun[d,e], A. Malizia[b], J. M. Mas-Hesse[g] M. Molina[a], L. Moran[a], M. Renaud[d,e], V. Sguera[a], S. E. Shaw[a,f], J. B. Stephen[b], R. Terrier[d,e], P. Ubertini[c], R. Walter[f], D. R. Willis[a,f], C. Winkler[h]

ABSTRACT

In this paper we report the second soft gamma-ray source catalog obtained with the IBIS/ISGRI gamma-ray imager on board the INTEGRAL satellite. The scientific dataset is based on more than 10 Ms of high quality observations performed during the first two years of Core Program and public IBIS/ISGRI observations, and covers ∼50% of the whole sky. The main aim of the first survey was to scan systematically, for the first time at energies above 20 keV, the whole Galactic Plane to achieve a limiting sensitivity of ∼1 mCrab in the central radian. The target of the second year of the INTEGRAL mission lifetime was to expand as much as possible our knowledge of the soft gamma-ray sky, with the same limiting sensitivity, to at least 50% of the whole sky, mainly by including a substantial coverage of extragalactic fields. This catalog comprises more than 200 high-energy sources detected in the energy range 20–100 keV, including new transients not active during the first year of operation, faint persistent objects revealed with longer exposure time, and several galactic and extragalactic sources in sky regions not observed in the first survey. The mean position error for all the sources detected with significance above 10σ is ∼40 arc seconds, enough to identify most of them with a known X-ray counterpart and to unveil the nature of

[a]School of Physics and Astronomy, University of Southampton, SO17 1BJ, UK

[b]IASF/INAF, Bologna, Italy

[c]IASF/INAF, Rome, Italy

[d]CEA-Saclay, DAPNIA/Service d'Astrophysique, F91191, Gif sur Yvette Cedex, France

[e]Federation de recherche APC, College de France 11, place Marcelin Berthelot, F75231, Paris, France

[f]Geneva Observatory, INTEGRAL Science Data Centre, Chemin d'Ecogia 16, 1291 Versoix, Switzerland

[g]Centro de Astrobiología (CSIC-INTA), E28850 Torrejón de Ardoz, Madrid, Spain

[h]ESA-ESTEC, Research and Scientific Support Dept., Keplerlaan 1, 2201 AZ, Noordwijk, The Netherlands

most of the strongly absorbed ones, even though they are very difficult to detect in X-rays.

Subject headings: gamma-rays: observations, surveys, Galaxy:general

1. Introduction

One of the key investigations of the INTEGRAL Observatory Core Programme has been the soft gamma-ray Galactic Plane Scans (hereafter GPS), successfully exploited during the first year of the mission lifetime to a depth of ∼1 mCrab in the central radian (Bird et al. 2004). The unprecedented sensitivity achieved in the gamma-ray domain over a ∼900 square degree field of view (FOV) was confirmed by the 'first survey results' (Ubertini et al. 2005a). The discovery of a soft gamma-ray sky populated with more than 120 sources was a stimulus for the INTEGRAL scientific community (i) to perform deeper exposures in the Galactic Plane region formerly covered with insufficient sensitivity, in particular regions out of the central radian, and (ii) to continue the strategy to perform several 'widely-scattered' high latitude observations dedicated to specific scientific objects, though providing the bonus of wide off-the-plane coverage (Winkler 2004). The ESA/INTEGRAL scientific policy to make all scientific data available to the public 1 year after the observation has allowed us to include high quality observations accounting for in excess of ∼10Ms exposure time in this iteration of the survey analysis.

2. The IBIS 'all sky' survey

In this paper we provide the second IBIS/ISGRI soft gamma-ray survey catalog, comprising more than 200 high-energy sources. As for the first catalog, the aim is to provide a prompt release of information to the community. The instrumental details and sensitivity can be found in Lebrun et al. (2003) and Ubertini et al. (2003), while the observation strategy and its technical implementation are summarised in Bird et al. (2004). The data are collected with the low-energy array, ISGRI (INTEGRAL Soft Gamma-Ray Imager; Lebrun et al. (2003)), consisting of a pixellated 128x128 CdTe solid-state detector that views the sky

[1]Based on observations with INTEGRAL, an ESA project with instruments and science data centre funded by ESA member states (especially the PI countries: Denmark, France, Germany, Italy, Switzerland, Spain), Czech Republic and Poland, and with the participation of Russia and the USA.

through coded aperture mask. IBIS/ISGRI generates images of the sky with a 12′ (FWHM) resolution and typical source location of better than 1′ over a $\sim 19°$(FWHM) field of view in the energy range 15–1000 keV. This 'all sky' catalog uses mosaic image data from the first 2 years of Core Program observations, including the Galactic Plane Scans (GPS), Galactic Center Deep Exposure (GCDE)and Pointed Observations from the first year of public data. The source fluxes are integrated over two energy bands (20–40 and 40–100 keV), and the limiting sensitivity for this survey is around 1 mCrab for the deepest exposures. While the first catalog provided coverage of the galactic plane only, this new catalog includes sources derived from a significantly larger dataset, with much better sky coverage. The dataset used in this catalog ensures that 50% of the sky is now observed with an exposure of at least 10ksec (see Figure 1).

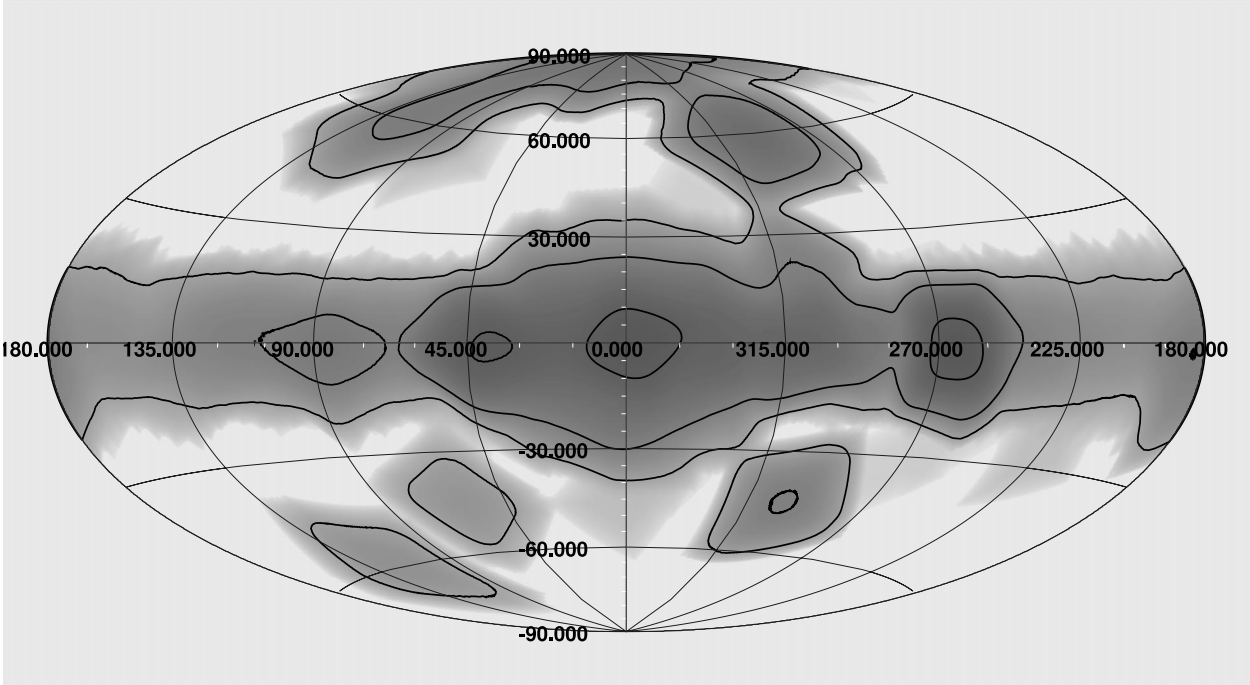

Fig. 1.— Exposure map for the second catalog observations. Contour levels are at 10, 100 and 1000 ksec.

3. Data analysis and catalog construction

3.1. Input dataset and pipeline processing

The survey input dataset consists of all data available at the end of September 2004, from revolutions (orbits) 46-209 inclusive, covering the time period from the completion of the performance and verification phase in February 2003 to the end of June 2004.

INTEGRAL/IBIS data is organised in short pointings (science windows) of ∼2000s. Pipeline processing was carried out using the standard *OSA 4.1* software up to the production of sky images for individual science windows. Ten adjacent energy bands (15–20, 20–30, 30–40, 40–60, 60–80, 80–100, 100–150, 150–300, 300–500 and 500–1000 keV) were used to allow later flexibility in data analysis.

Construction of an input catalog is a key part of the use of *OSA* imaging software. The optimal input catalog should contain all sources which may be visible in individual science windows, and hence will require cleaning from images, with very accurate positions. The final input catalog used in the image processing was a list of ∼400 excesses produced primarily by a preliminary processing of the dataset using *OSA 4.0* and an input catalog based on the first IBIS/ISGRI survey. The following constituted the final input cleaning catalog:

- All sources listed in the first IBIS/ISGRI catalog
- All other IGR sources detected and published up to the start of processing
- All excesses above a significance limit of 4.5σ detected in preliminary *OSA 4.0* mosaics.
- A list of additional transient sources obtained by searching preliminary *OSA 4.0* science window images.

3.2. Science window selection

It was observed that some science window pointing images were of poor quality, and therefore would have resulted in degraded image quality if added into the final mosaics, so these were removed prior to mosaic construction. The criterion used to remove these poorer quality images was the overall image rms statistic. A histogram of image rms (Figure 2) shows a broad population of 'good' images, but also a number of outliers. Inspection of these anomalous science windows indicated that they were almost always associated with areas of high background (at the beginning or end of an orbit, or following solar flares) or

the presence of a bright source near the edge of the IBIS partially coded FOV. Since the final image rms is a clear function of the energy band, the allowed rms range was determined independently for each energy band, ultimately requiring the rejection of $\sim 5\,\%$ of the science windows. In addition, any science windows acquired in 'staring' mode were removed due to their adverse effect on final mosaic quality.

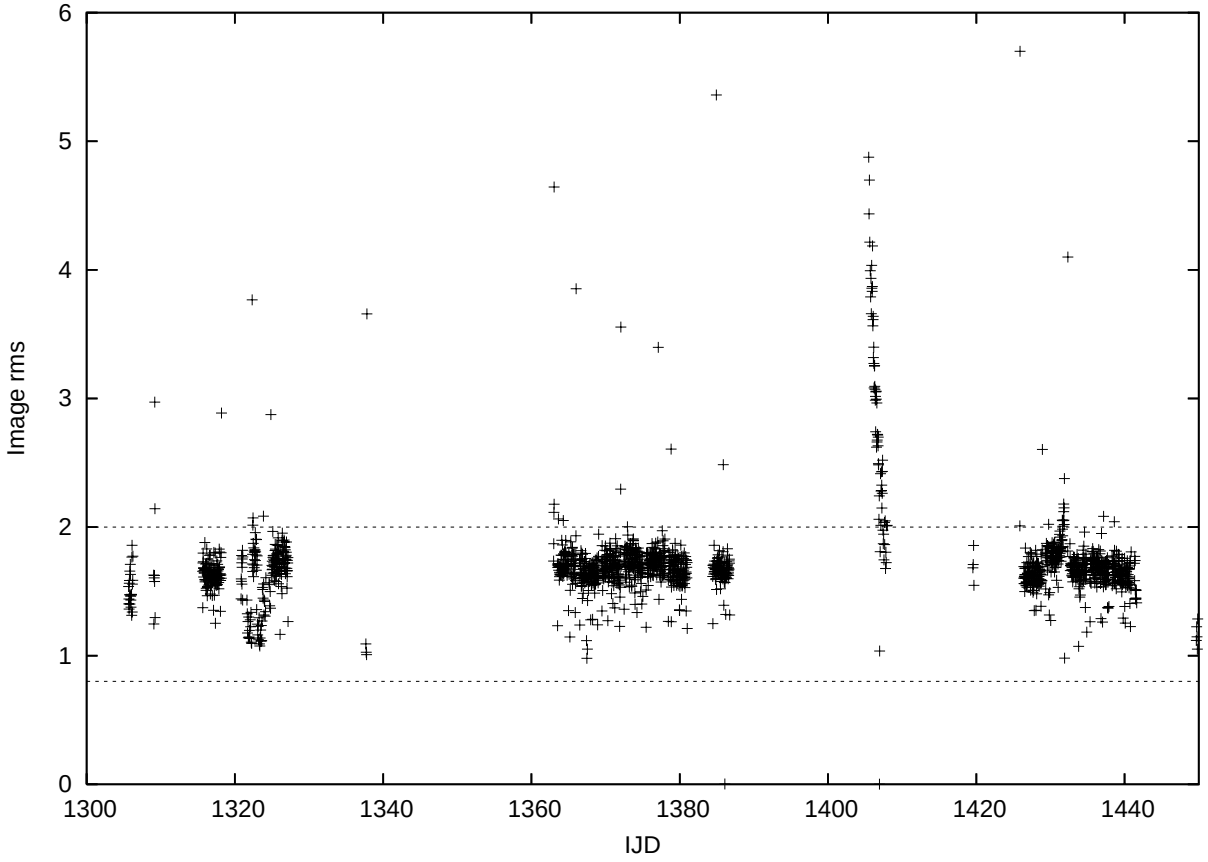

Fig. 2.— Image rms as function of time (each point represents one scw) for the 40-60 keV science-window images. The decaying rms at IJD∼1410 shows the recovery of the instruments after the massive solar flare of Oct 28th 2003. The dashed lines represent the acceptance limits applied during scw filtering.

3.3. Mosaicing

The selected science windows were mosaiced using a proprietary tool optimised to create all-sky galactic maps based on several thousand input science windows.

Mosaics were produced for the whole dataset for each of the narrow energy bands indicated in Section 3.1, and additionally for the following broad bands: 20-40, 30-60, 20-60, 20-80, 20-100 keV. The 20-40 and 30-60 keV bands were intended as primary search bands as the highest image quality is seen in this regime. However, previous investigation indicated that broader bands such as 20-100 keV are better suited for searches for extragalactic objects. Each mosaic covered the whole-sky area with an equal-area projection with a pixel size of 0.06° ($3.6'$) at the centre of the mosaic.

Additional mosaics were made for each revolution (in the 20-40 keV band) and for each GCDE period (in the 20-100 keV band) covered by the dataset.

3.4. Source searching and location

Each of the mosaics was searched using the *SExtractor 2.3.2* software (Bertin & Arnouts 1996). In practice, the AITOFF projection used for all-sky images introduces heavy distortion to the PSF of sources with $|b| > 60^\circ$, so additional maps were made using polar (ARC) projections to enable more effective searching, and location, of sources in the galactic polar regions. The source positions measured by *SExtractor* represent the centroid of the source calculated by taking the first order moments of the source profile (referred to by *SExtractor* as the barycenter method).

Source detectability is limited at the faintest levels by background noise and can be improved by the application of a linear filtering of the data. In addition, source confusion in crowded fields can be minimised by the application of a bandpass filter. To this end, the *mexhat* bandpass filter is used in the *SExtractor* software. The convolution of the filter with the mosaic alters the source significances, hence *SExtractor* uses the source positions identified from the filtered mosaic to extract the source significances from the original mosaic.

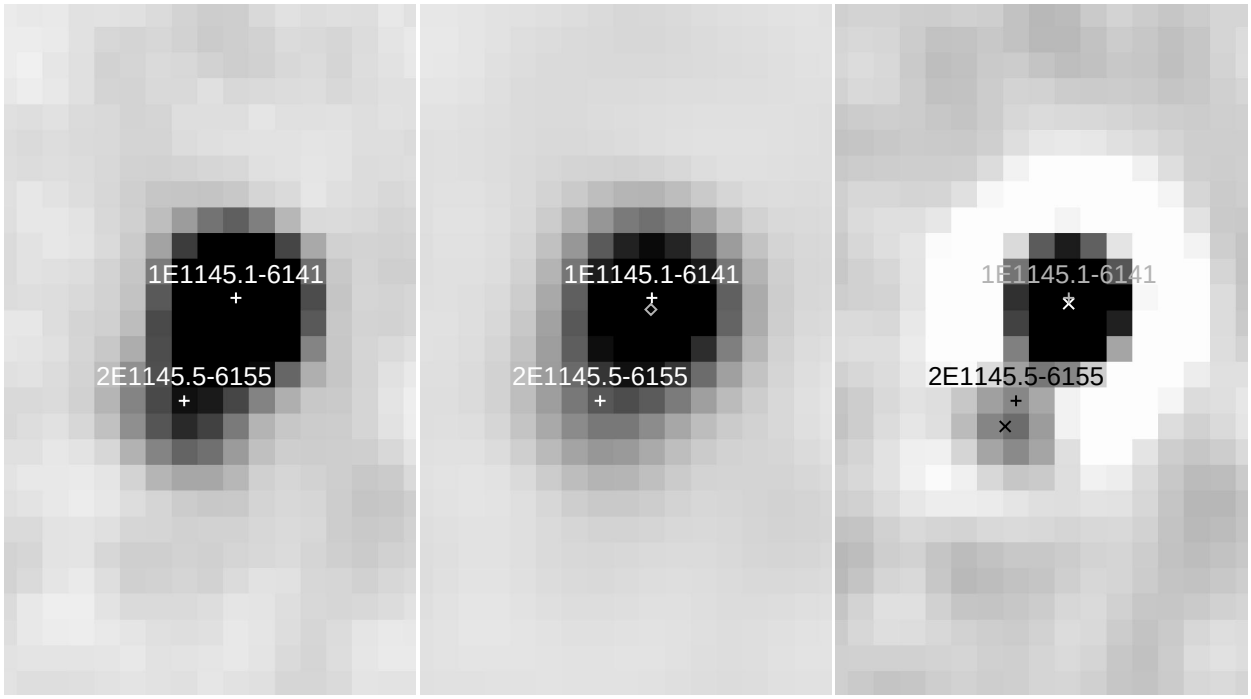

Fig. 3.— Results of *SExtractor* application to a region containing the blended sources, 1E 1145.1-6141 & 2E 1145.5-6155. *Left*: The region in the original 20-60 keV mosaic. *Middle*: The region in the gaussian-filtered 20-60 keV mosaic. *Right*: The region in the bandpass-filtered 20-60 keV mosaic. The diamond symbol represents the source position found using a Gaussian filter; the x symbols represents the source positions found by the *mexhat* filter; the + symbols indicate the SIMBAD source locations.

Figure 3 demonstrates the efficiency of the bandpass filter in separating sources in close proximity, in this case 1E 1145.1-6141 and 2E 1145.5-6155, with an angular separation of ∼15', close to the angular resolution of the telescope. If we use a simple Gaussian filter, *SExtractor* identifies only a single extended source indicated by the diamond symbol located close to the brighter emission. In comparison, the application of the *mexhat* filter provides detection of both sources, even though the position of the weaker source, 2E 1145.5-6155, is shifted ∼1 pixel (3.6′) away from the expected SIMBAD location of the source.

3.5. Source list filtering

An initial list of 1019 excesses was generated by integration of all lists derived from mosaic images on whole-archive and by-revolution timescales.

To identify at what significance these excesses represent 'real' sources, and are not attributable to the statistical and systematic background noise distribution, a type of 'LogN-LogS' plot was created for each of the broad energy bands that were searched for sources. The significance of each excess found by *SExtractor* in a mosaic was plotted against the number of excesses having that significance or greater. This is shown in Fig. 4 for the 30-60 keV significance mosaic. The dash-dot line represents a combined Gaussian and power-law model; the dashed line represents the power-law component of the model; and the dotted line the Gaussian component used to approximate the noise. Using these plots, the significances at which the noise components dominated each map could be estimated and only sources above this threshold, formally defined as the point above which at most 1% of the excesses may be false detections, were considered.

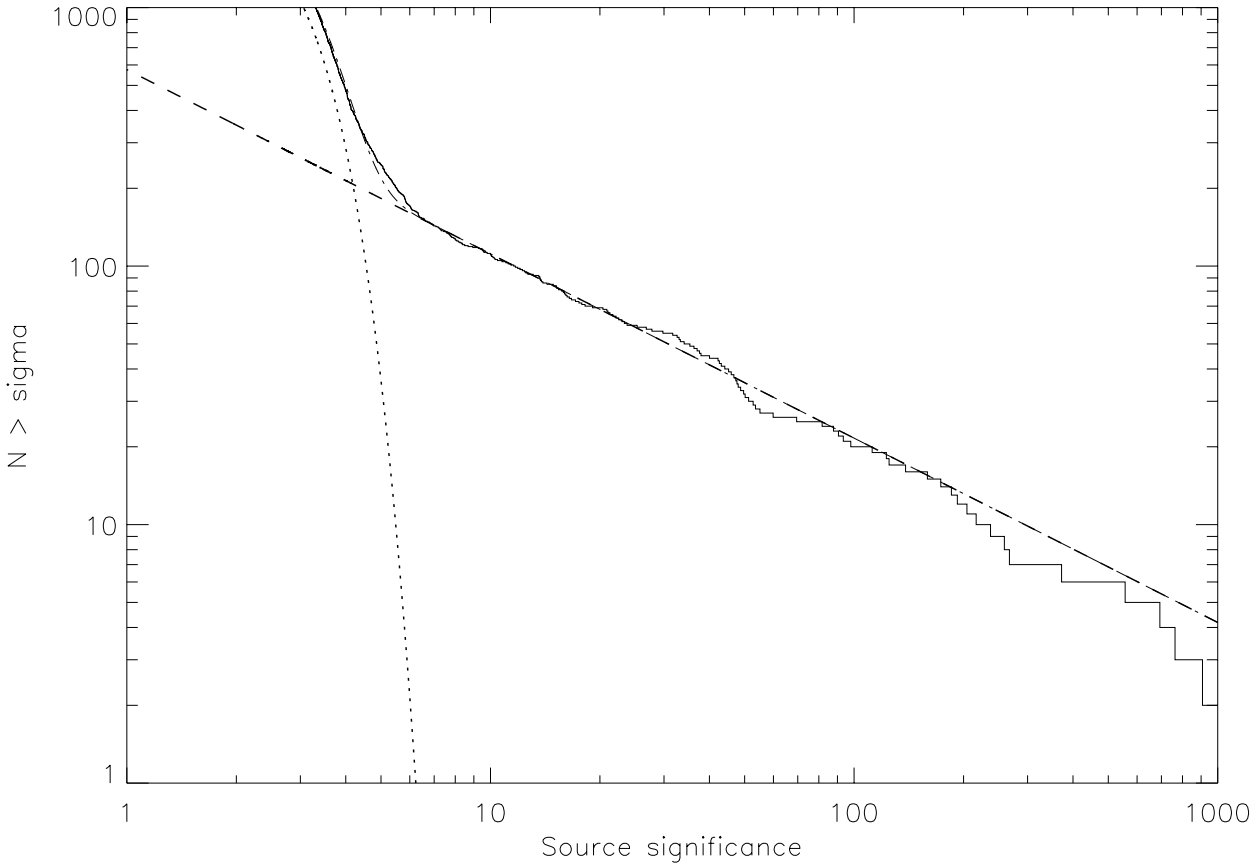

Fig. 4.— Distribution of significances of source-like excesses found in the 30-60 keV all-sky mosaic. The solid line represents the data; see the text for discussion of the individual fits displayed.

The thresholds thus derived were $5.5\,\sigma$ in the 20-40 keV band, $5\,\sigma$ in the 30-60 keV and 20-100 bands, and $6\,\sigma$ in a single revolution mosaic. All excesses above any of these thresholds were then combined into a preliminary source list, and merged with two additional independent source lists based on either spatial or temporal subsets of the whole survey data. The resulting candidate sources were first inspected visually to ensure an appropriate point spread function. In those cases where an excess was in an area of the map containing structure, sources were both visually verified and required to have a significance at least $3\,\sigma$ higher than any non-statistical background features within a few degrees radius. After all selection processes, we obtain a source list containing 209 sources, as shown in Table 2.

3.6. Galactic Centre Localizations

The final survey images used for the second catalog are mosaics of revolutions 46 to 209 and as such do not truly represent all of the sources ISGRI has detected in the Galactic Centre Region (GCR). This region contains many highly variable sources in a small area of sky ($\sim 2^\circ \times 2^\circ$), leading to a high degree of source confusion and positional uncertainty. The Galactic Centre was observed in 33 revolutions of the survey data used in this catalog. In the final mosaic, the GCR appears as a 'blend' of sources, impossible to resolve into its constituents. However, the GCR sources are seen to vary in brightness from revolution to revolution (Figure 5). By exploiting their highly variable nature, most sources could be de-blended by analysing the individual revolution ($\sim$3 day) mosaics. For example, SLX 1744-299 was present in all but 9 of the 33 revolutions, while SAX J1747.0-2853 appeared only in revolution 175.

Bélanger et al. (2004) reports the positions of 6 sources located in the $2^\circ \times 2^\circ$ region surrounding the Galactic Centre, as seen with ISGRI during April/May 2003 and determined from 20-40 keV and 40-100 keV mosaics of 850 ksec total effective exposure, using a simultaneous PSF fit of sources in the GCR. This, combined with the more isolated sources seen in our own mosaics, represents our best prior knowledge of the hard X-ray emitters in the Galactic Centre.

To de-blend this region, each revolution mosaic (in the 20-40 keV band) covering the Galactic Centre region was visually inspected in turn, noting the coordinates of excesses in the GCR in each revolution. By combining the positions obtained in this way, ten distinct sources could be identified, including all 6 sources detected by Bélanger et al. (2004). See Table 1 for the GCR source list.

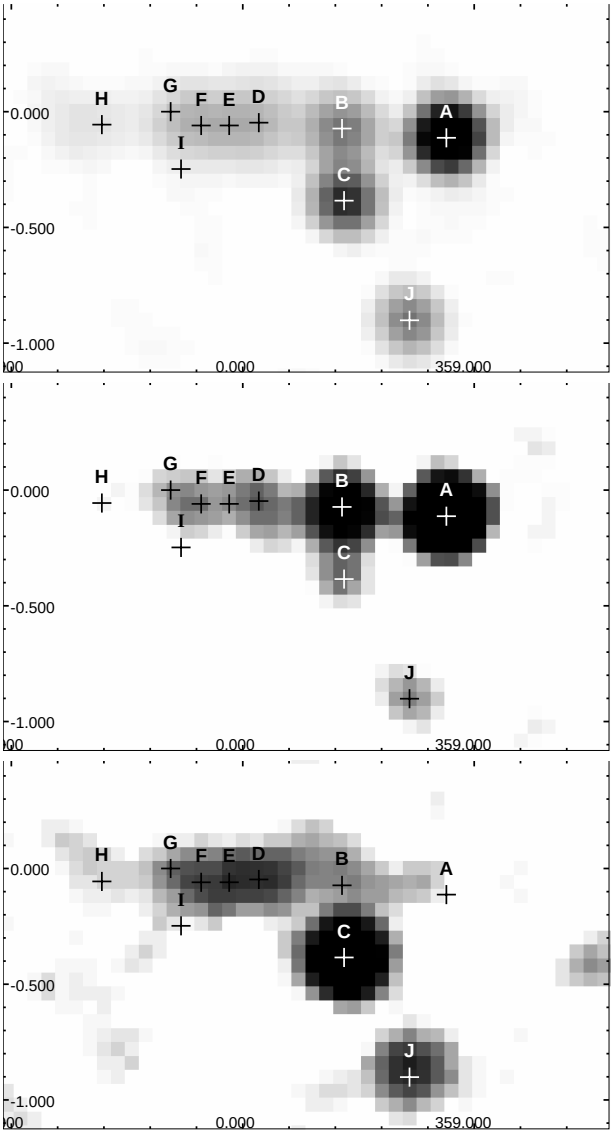

Fig. 5.— (top) the final mosaic for the Galactic Centre, showing the confused nature of the region; (centre) map for revolution 53; (bottom) map for revolution 183. All maps show flux in the 20–40 keV band. See Table 1 for source identifications.

Table 1: Sources extracted from Galactic Centre region by spatial and temporal de-blending

ID	Source Name	(RA,Dec)	N_{rev}[†]	Notes
A	IE 1740.7-2942	(265.988,-29.745)	21	2, b
B	KS 1741-2931	(266.220,-29.340)	19	1(53), b
C	1A 1742-294	(266.520,-29.510)	18	2,b
D	IGR J17456-2901	(266.410,-29.020)	9	2,4,b
E	1E 1742.8-2853	(266.498,-28.917)	13	3
F	1E 1742.9-2849	(266.570,-28.814)	7	3
G	1E 1743.1-2843	(266.590,-28.670)	4	2,b
H	IGR J17475-2822	(266.820,-28.445)	6	1(119,120)
I	SAX J1747.0-2853	(266.805,-28.837)	1	1(175)
J	SLX 1744-299	(266.860,-30.020)	29	2,b

[†]Number of revolutions in which source is detectable

[b]presented in Bélanger et al. (2004)

[1]Position taken from one revolution (revolution number)

[2]Centroid of positions from individual revolutions that are consistent with Bélanger et al. (2004)

[3]Could not be de-blended, SIMBAD coords used

[4]Coincident with Sgr A*, but not unambiguously identified

The centroids of these positions (determined from the individual revolutions) were compared with the coordinates of the 6 sources quoted by Bélanger et al. (2004). Our coordinates were found to be consistent for 5 sources, the exception being KS 1741-293. This source is particularly bright and well defined in revolution 53 and therefore the coordinates were derived from this image (the position in Belanger et al. is quoted as being 2.31′ from the nominal position for this source, while our position has an offset of 1.34′). This method was also used for two of the remaining sources (not detected by Belanger et al.): IGR J17475-2822 (well defined in revolutions 119 and 120); and SAX J1747.0-2853 (only seen in revolution 175). Finally, 1E 1724.8-2853 and 1E 1742.9-2849 could not be sufficiently de-blended, so coordinates from existing catalogs were used.

3.7. Flux extraction

Time-averaged fluxes were extracted by generating a light curve for each source, taking into account all science windows in which the source was within the field of view. A weighted mean was generated for each light curve, which provides a flux estimate which is, in principle, identical to that obtained in the mosaics, but which is found in practice to be more robust against distortions of the mosaic and small losses seen in the mosaicing algorithm.

Light curves, and hence fluxes, were generated in the 20-40 and 40-100 keV energy bands; these allow an approximate assessment of the spectral characteristics of each source to be made.

Fluxes and further analysis of those sources emitting at higher energies will be provided in an additional catalog (Bazzano et al. 2005).

4. Data Quality

4.1. Positions

The astrometric coordinates of the source positions were extracted from the mosaics by the barycentring routines built into *SExtractor 2.3.2*. Of the 209 sources listed in the 2^{nd} IBIS/ISGRI catalog, 179 have well-defined positions obtained in different wavebands according to the SIMBAD/NED database. Measuring the angular distance between the measured positions and those provided by the SIMBAD database gives an indication of the source position errors. The mean position error of all sources detected at a 10σ level or higher is $\sim 0.7'$. However, the point source location error of IBIS is highly dependent upon

the significance of the source detected (Gros et al. 2003).

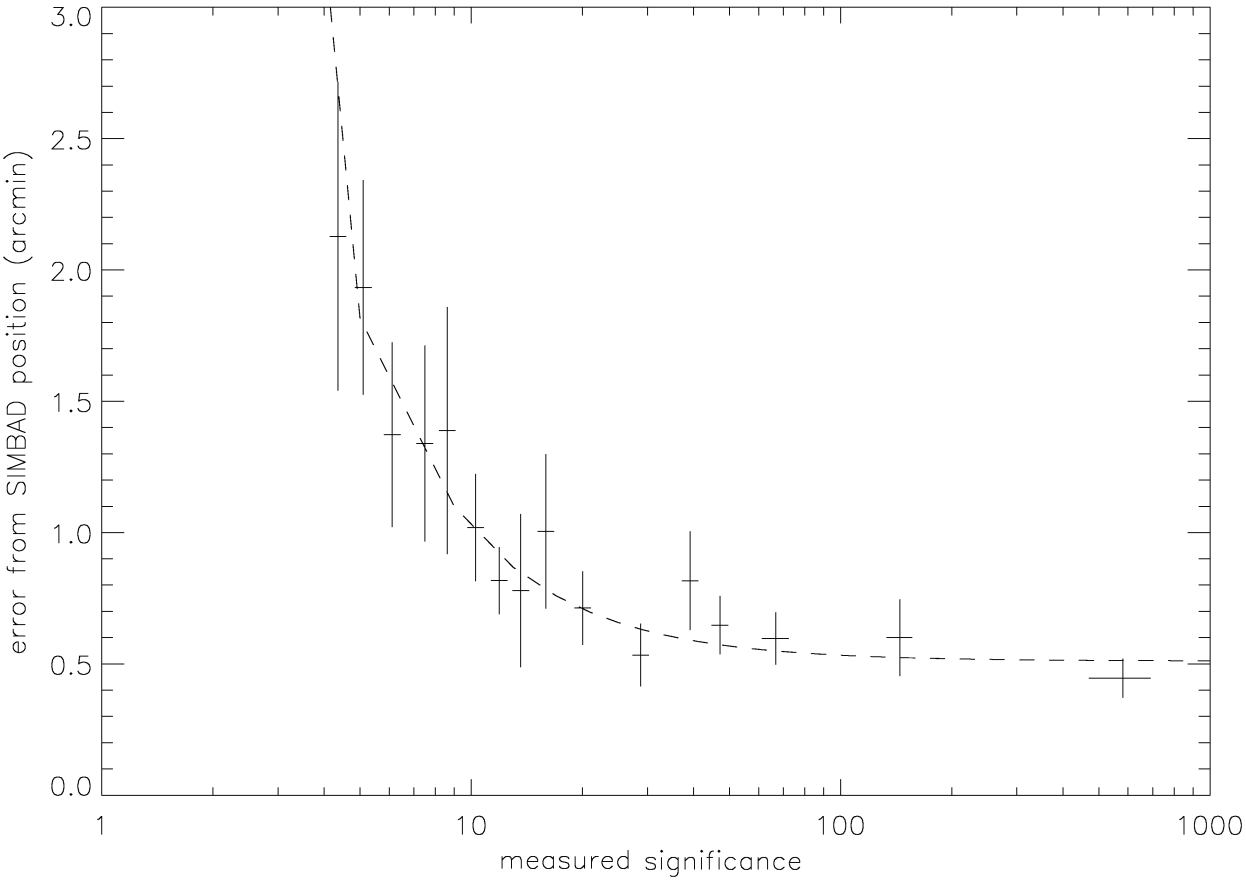

Fig. 6.— The binned mean source position error of sources as a function of source significance. Each bin contains 10 sources. The dashed line indicates the model shown in Equation 1.

By binning together sources of similar significance and calculating the mean source position error we can see how the source positioning accuracy varies with significance; this is shown in Fig. 6. The data is fit by a power-law model with a constant offset:

$$\delta x = 11.6 S^{-1.36} + 0.51 \quad (1)$$

where δx is the error in the source position (in arc minutes) and S is the source significance. This indicates that for the most significant detections we do not, on average, obtain a source location better than $0.51'$. For sources which have a significance of $\sim 5\sigma$ we have a mean accuracy of $< 2'$.

Gros et al. (2003) gives the range of the 90% confidence level error radius as $3'$ – $20''$, with an error better than $1'$ for $\sigma > 30$, and they note that these results are derived from fields with few detected sources and may not be accurate in crowded fields. The source location accuracy of the source positions in the 2^{nd} IBIS/ISGRI catalog is better than predicted by Gros et al. (2003) with an error better than $0.7'$ for $\sigma > 10$.

4.2. Source fluxes

The majority of the soft gamma-ray sources detected by IBIS are intrinsically variable. Furthermore, the transient sources also exhibit outburst or flaring activity due to their binary nature coupled with accretion-driven processes. For this reason, since the fluxes quoted are an average over two years of observations, we cannot expect a strong agreement between the fluxes of the two catalogs. Moreover, we have made a substantial improvement in our understanding of the instrument and the software used to extract the scientific data in order to better take account of the systematic effects present. The fluxes derived in the first catalog used an earlier version of the *OSA* imaging software, which has been upgraded in many areas, and specifically in terms of the off-axis response corrections available in *OSA 4.0* onwards. For survey data, where we combine multiple pointings at various off-axis angles, this is critical, and the lack of off-axis corrections in *OSA 3* would have created a systematic underestimate of the fluxes in the first catalog. Use of the light-curve extraction method also removes any flux losses during the mosaicing process, which we estimate at ∼4-6% for the mosaics used in the first catalog compilation.

5. Discussion

We have derived an 'unbiased' catalog of 209 sources observed in a systematic analysis of the IBIS/ISGRI Core Programme and public data spanning nearly 2 years of operation. Figures 7-9 show significance maps in the 30–60 keV energy band for 30° sections of the Galactic plane.

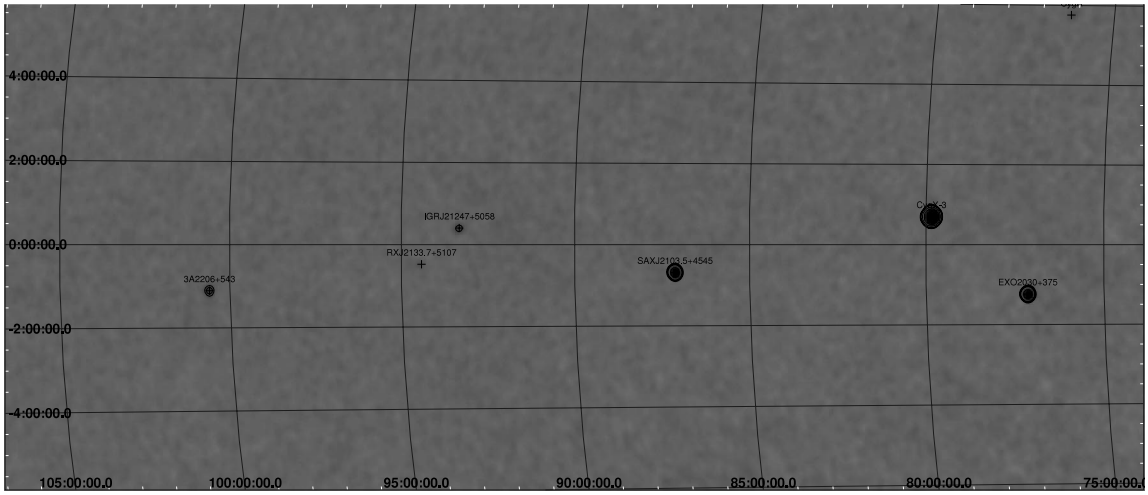

Fig. 7.— 30-60 keV sky-maps covering 30° sections of the Galactic Plane

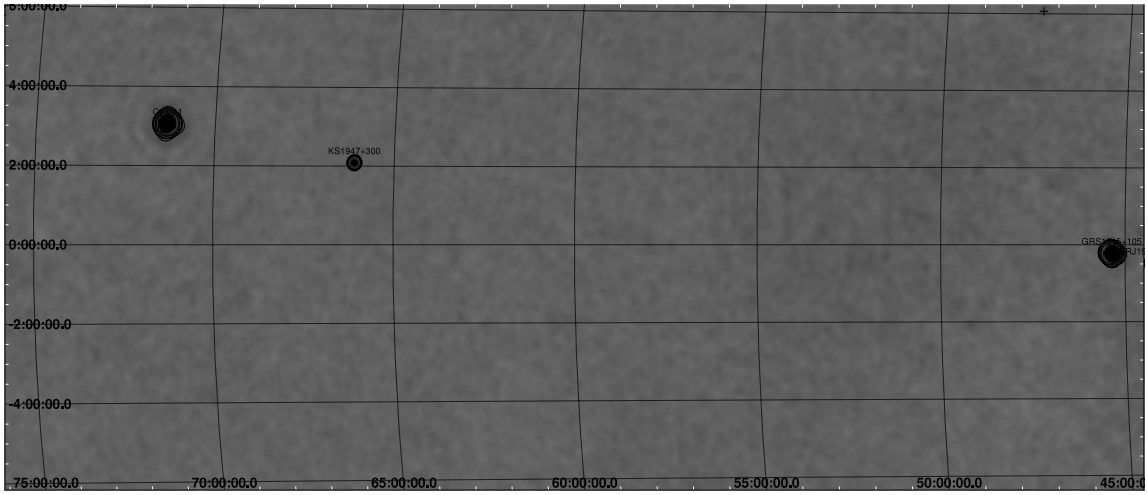

Fig. 7.— continued.

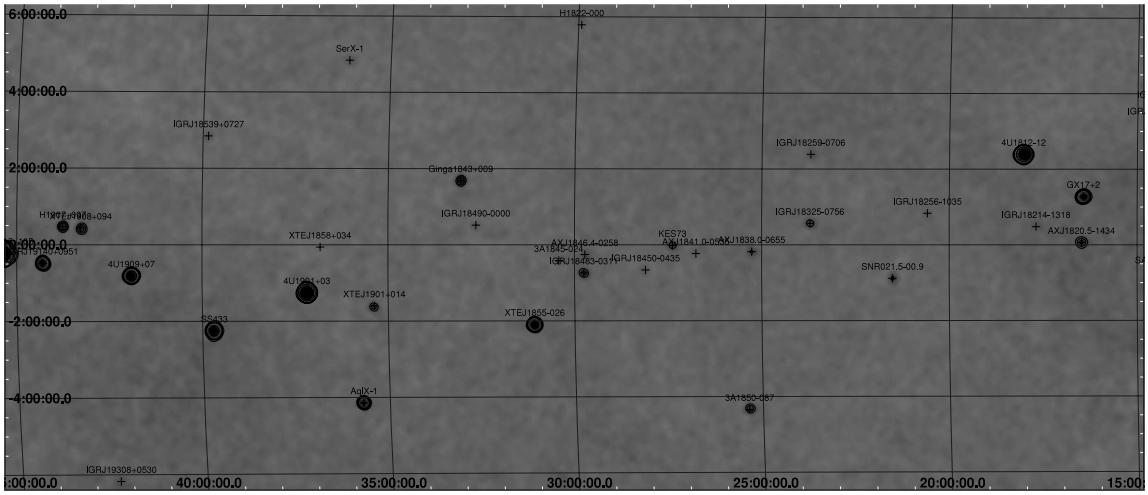

Fig. 7.— continued.

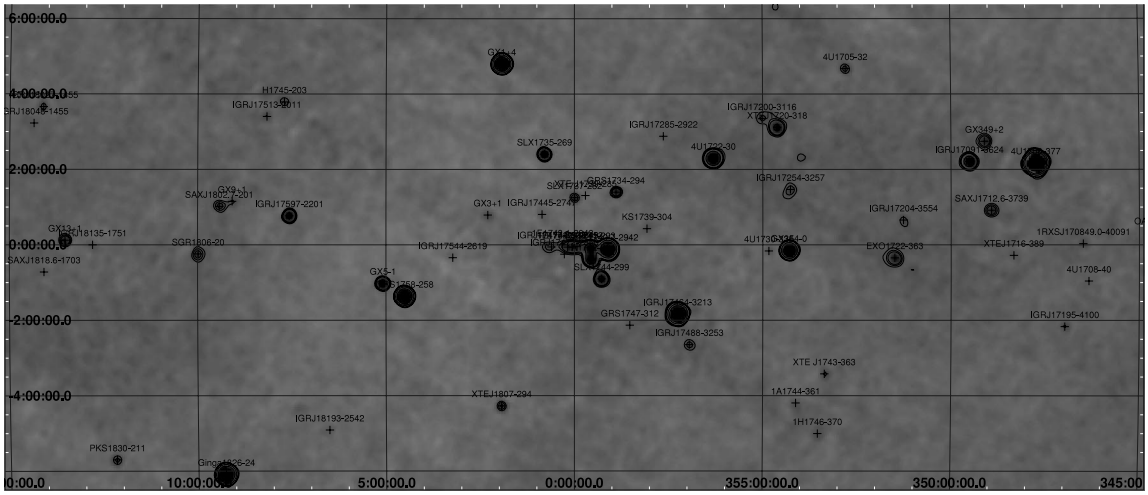

Fig. 8.— 30-60 keV sky-maps covering 30° sections of the Galactic Plane

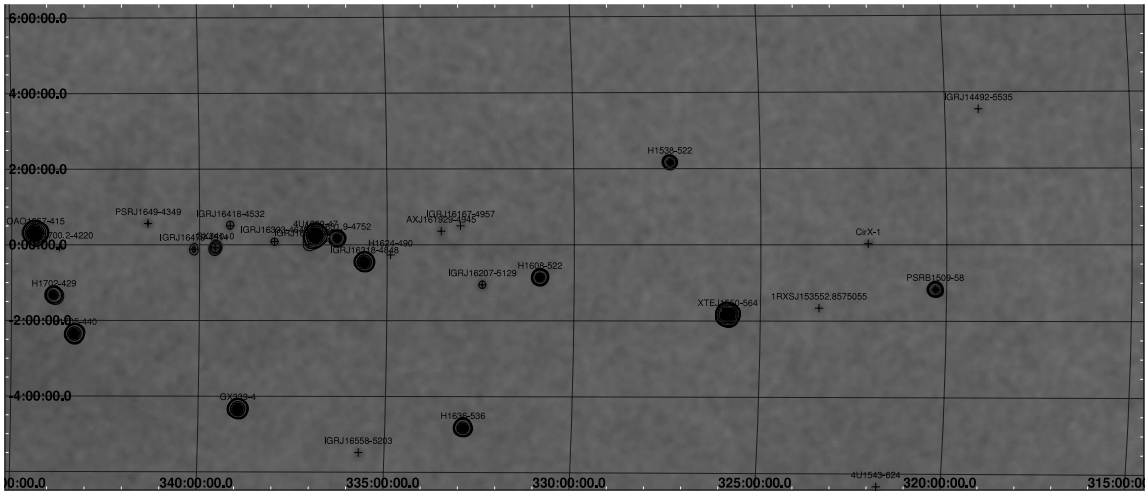

Fig. 8.— continued.

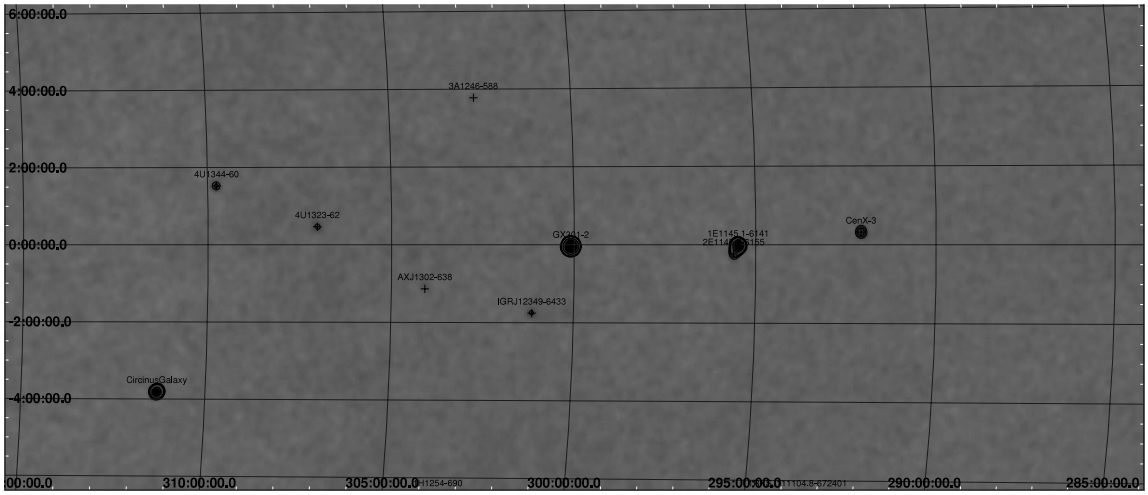

Fig. 8.— continued.

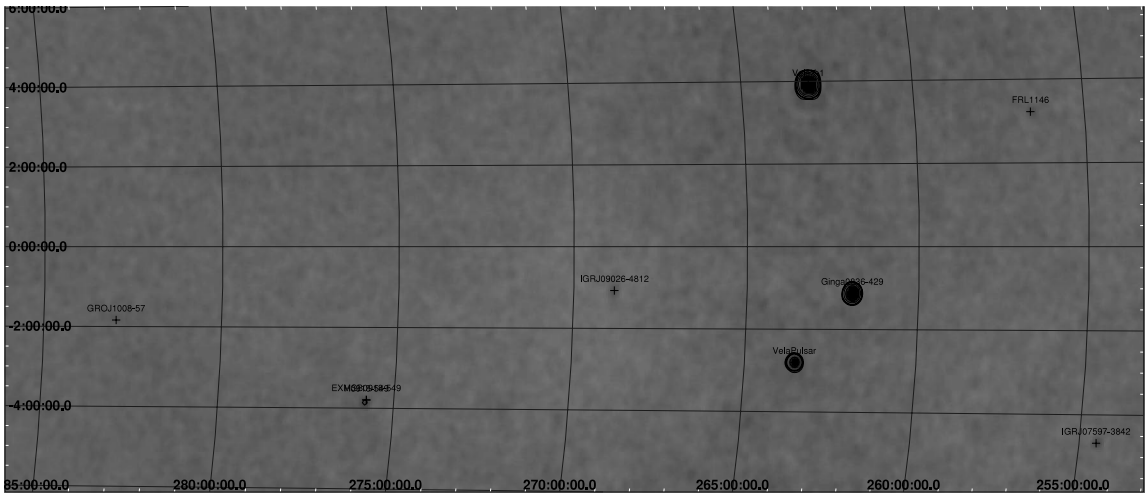

Fig. 9.— 30-60 keV sky-maps covering 30° sections of the Galactic Plane

The last year has seen a substantial improvement in our understanding of the instrument and software, and hence our detection of sources. Improvements to the off-axis responses, and better flux extraction tools have allowed us to produce more reliable flux estimates, albeit for time-averaged fluxes which are only indicative of brightness for the highly variable sources which dominate the high-energy sky.

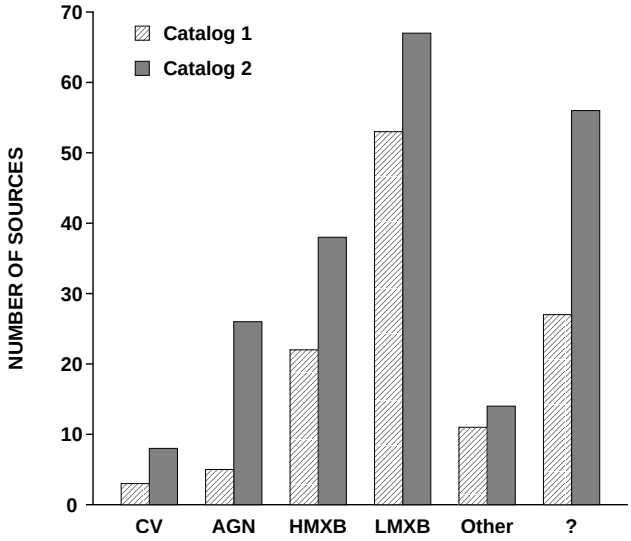

Fig. 10.— Numbers of sources in the 1st and 2nd IBIS/ISGRI catalogs, classified by type.

Figure 10 illustrates a simple breakdown of the 209 sources presented in this catalog by source type, and how this breakdown compares to the first catalog. The source list remains dominated by Galactic accreting binaries: a total of 113 objects, represented by 38 high-mass and 67 low-mass X-ray binaries (HMXB and LMXB respectively), but also a small population of cataclysmic variables (CVs). In most cases, the compact object is a neutron star (79 confirmed cases; 32 in HMXB, 47 in LMXB) but the sample also contains 4 confirmed black holes (1 in HMXB and 3 in LMXB) and 6 LMXB black hole candidates (BHC). There is an additional 4 tentative associations as BHCs, based simply on the spectral and temporal characteristics of the sources. Also worthy of note is our detection of IGR J1745.6-2901, shown to be coincident with supermassive black hole candidate Sgr A* (Bélanger et al. 2004). The Galactic sample also includes 4 isolated pulsars (one of which is an anomalous X-ray pulsar, AXP), 4 supernova remnants (of which 2 are associated with AXPs) and two associations with molecular clouds.

As a direct consequence of the wider and deeper sky coverage (see Figure 1), there has been a five-fold increase in AGN detections over the first catalog. The improved sky coverage has provided us with a first real look at the extragalactic sky with IBIS, detecting 33 extragalactic sources (close to ∼20% of the entire catalog), of which there are: 2 clusters of galaxies; 22 Seyfert galaxies; 3 blazars and 6 more sources whose classifications are unconfirmed but are coincident with AGN. Further analysis of this sample will be presented in Bassani et al. (2005)

Compared to the first IBIS/ISGRI catalog, the number of detections without a firm classification has doubled, but this represents a similar proportion of the total number of sources (∼25%) as in the first. Of the unclassified sources, 39 are of an unknown nature, while the remaining 17 have unconfirmed, so called 'tentative' classifications. Approximately one quarter of the sources cataloged as unclassified in the first catalog have now been classified - 3 HMXB, 1 LMXB, 1 CV and 2 AGN with many more tentative associations. The majority (∼80%) of the remaining and new unclassified sources are INTEGRAL discoveries.

INTEGRAL Gamma-ray (IGR) sources, represent detections that are either entirely new or those with no obvious counterpart or association in the hard X-ray and/or gamma-ray wavebands. There is a total of 56 IGRs in the second catalog (double that of the first catalog), of which 20% have been classified (see Figure 11). This percentage increases to ∼40% if the tentative classifications are included. Looking at the IGR sources broken down by source type, it is interesting to note that nearly half of the cataloged CVs are IGR sources, while <5% of the cataloged LMXBs and HMXBs are INTEGRAL discoveries, although this number increases to nearly 10% if the tentative associations are included.

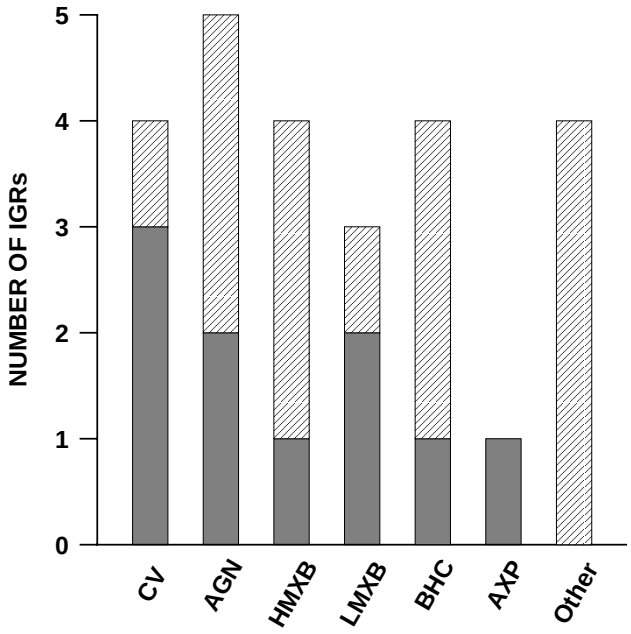

Fig. 11.— Classifications of IGR sources. Solid bars indicate numbers of IGRs with firm classifications (note that sources can be in more than one category). Hatched bars show tentative classifications).

A full understanding of the nature of the new sources, and their classifications in the already known classes of high energy emitters, is a challenging task, and is triggering a strong follow-up program at all wavelengths.

The catalog by Macomb & Gehrels (1999) provides the previous reference for sources detected above 50 keV by at least one experiment. It contains a general list of basic characteristics for 309 sources and summary tables of different observations of sources by object classification. Of the 309 sources, 183 have been detected only for energies above 1 MeV and 135 are unidentified (the majority of which are EGRET detected sources). The remaining 126 sources are categorised as 83 accreting sources, 22 Seyfert galaxies, 14 gamma-ray blazars, 7 gamma-ray pulsars, 6 clusters or galaxies and 3 SNR. By comparison, this second IBIS/ISGRI catalog is reaching a similar level of coverage for Galactic sources, although interestingly the blazar population is so far largely unseen, due to the relatively low energy band of the IBIS/ISGRI observations.

The following sources, included in the first catalog, are no longer listed: 1E 1742.5-2859 and 1E 1742.9-2929 have been replaced by other sources following a more in-depth analysis of the source contributions in the Galactic centre region (see Section 3.6); IGR J17460-3047 was found to be an artefact of the earlier imaging process used in the first catalog.

5.1. Concluding comments

The positions deriving from ISGRI are forming the basis for an active program of follow-up observations in other wavebands, mainly X-ray (XMM-Newton, Chandra and RXTE), optical, IR and radio. Of particular interest are the recent correlations with the new population of very high-energy gamma-ray sources detected in the Milky Way by the HESS consortium, and emitting in the 0.2-10 TeV range (Aharonian et al. 2005). At least two new IBIS sources are firmly associated with this new class of high-energy accelerator (Ubertini et al. 2005b; Malizia et al. 2005).

The IBIS survey team, including scientists from five different institutes, will continue to refine the analysis techniques and apply them to the ever-increasing IBIS dataset. Further catalogs are expected to be released at regular yearly intervals. Based on our current sky coverage, the observed source log N-log S (Dean et al. 2005) and projected observation plans, we conservatively estimate the final number of sources will be over 500. In particular, in the coming months, we can expect the exposure in the extragalactic sky to improve significantly, allowing us to explore previously unexposed regions of the hard X-ray sky.

Finally, we also note that after the successful launch of the Swift satellite on November

20 2004, ISGRI is no longer the sole instrument capable of surveying the sky in the hard X-ray band. The Burst Alert Telescope (BAT) onboard Swift (Gehrels et al. 2004; Barthelmy et al 2004) is a wide field of view (1.4 sr FWHM) coded mask instrument imaging in the 15–150 keV range. Although operating primarily as a GRB detector, it also acts as an all-sky monitor in the hard X-ray band. Due to the wide field of view the background is comparatively much higher than ISGRI, but with the increased exposure to the sky and the larger detector area (5240 cm^2) it has a comparable performance as a surveying instrument. However, the operating principles of the two instruments is very different. INTEGRAL is involved in a scheduled observation plan biased on the galactic plane as shown in Figure 1, whereas BAT is pointed randomly across the sky and so the differences in emphasis between the observation plans will cause the two instruments to complement each other well. Areas of low galactic latitude (especially the Galactic Centre) will be better covered with ISGRI whereas the even coverage of the BAT will mean that areas of high galactic latitude will be better covered by that instrument. There is therefore excellent complementarity between the two instruments and the surveys they will produce in the coming years.

We acknowledge the following funding: in Italian Space Agency financial and programmatic support via contracts I/R/046/04; in UK via PPARC grant GR/2002/00446; in France, we thank CNES for support during ISGRI development and INTEGRAL data analysis. This research has made use of: data obtained from the High Energy Astrophysics Science Archive Research Center (HEASARC) provided by NASA's Goddard Space Flight Center; the SIMBAD database operated at CDS, Strasbourg, France; the NASA/IPAC Extragalactic Database (NED) operated by the Jet Propulsion Laboratory, California Institute of Technology, under contract with the National Aeronautics and Space Administration.

REFERENCES

Aharonian, F., Akhperjanian, A. G., Aye, K.-M. et al. 2005, A&A, 435, L17-L20

Arnaud, K. A., Johnstone, R. M., Fabian, A. C., et al. 1987, MNRAS, 227, 241

Atteia, J.-L., Boer, M., Hurley, K., et al. 1987, ApJ, 320, 105

Augello, G., Iaria, R., Robba, N. R., et al. 2003, ApJ, 596, 63

Bamba, A., Yokogawa, J., Ueno, M., et al. 2001, PASJ, 53, 1179

Barlow, E.J., Bird, A.J., Clark, D.J., et al. 2005, A&A, 437, L27.

Barthelmy, S.D. 2004, Proc. SPIE, 5165, 175.

Bassani, L., et al., in preparation.

Bassani, L., et al., ATEL # 537.

Bazzano, A., et al., in preparation.

Bélanger, G., Goldwurm, A., Goldoni, P., et al. 2004, ApJ 601, L163

Bertin, E. & Arnouts, S. 1996, A&AS, 117, 393

Bird, A.J., Barlow, E.J., Bassani, A., et al. 2004, ApJ, 607, 33

Combi, J. A., Ribo, M., Mirabel, I. F., et al. 2004, A&A, 422, 103

Cowley, A. P., Crampton, D., Hutchings, J. B., et al. 1987, AJ, 93, 195

Davelaar, J., Smith, A., & Becker, R.H. 1986, ApJ, 300, 59

Dean A.J., et al., accepted for publication in A&A.

Dermer, C. D., & Gehrels, N. 1995, ApJ, 447, 103

Done, C., Madejski, G. M., Smith, D. A., et al. 1996, ApJ, 463, 63

Downes, R.A., Webbink, R.F., Shara M.M., et al. 2001, PASP, 113, 764

Ebeling, H., Mullis, C.R., and Tully, R.B. 2002, ApJ, 580, 774.

Forman, W., Jones, C., Cominsky, L., et al. 1978, ApJS, 38, 357

Gaensicke, B. T., Marsh, T. R., Edge, A., et al. 2005 ATEL # 63

Galloway, D. K., Remillard, R., Morgan, E., et al. 2003, IAU Circ. 8081

Gehrels, N., Chincarini, G., Giommi, P., et al. 2004, ApJ, 611, 1005.

Gonzalez-Riestra, R., Oosterbroek, T., Kuulkers, E., 2004, A&A, 420, 589

Gotthelf, E.V., & Vasisht G. 1998, NewA, 3, 293

Grebenev, S. A., Bird, A. J., Molkov, S. V., etal. 2005 ATEL # 457

Gros, A., Goldwurm, A., Cadolle-Bel, M., et al. 2003, A&A, 411, L179

Haberl, F., Motch, C., & Zickgraf, F.-J., 2002, A&A, 387, 201

Harmon, B. A., Wilson, C. A., Fishman, G. J., et al. 2004, ApJS, 154, 585

Hill, A.B., Walter, R., Knigge, C., et al., 2005, A&A, 439, 255

Laurent, P., Paul, J., Claret, A., et al. 1994, A&A, 286, 838

Lebrun , F., Leray, J.P., Lavocat, P., et al. 2003, A&A, 411, L141

Levine, A. M., Rappaport, S., Remillard, R., et al. 2004, 617, 1284

Liu, Q.Z., van Paradijs, J., van der Heuvel, E.P.J., et al. 2000, A&AS, 147, 25

Liu, Q.Z., van Paradijs, J., van der Heuvel, E.P.J., et al. 2001, A&A, 368, 1021

Lutovinov, A., & Revnivtsev, M. 2003, Astron. Lett. 29, 719

Lutovinov, A., Rodriguez, J., Revnivtsev, M., et al. 2005, A&A, 433, 41

Lutovinov, A., Revnivtsev, M., Molkov, S., et al. 2005, A&A, 430, 997

Macomb, D.J., & Gehrels, N., ApJ Suppl., 120, 335.

Malizia, A., Bassani, L., Di Cocco, G., et al. 2004, ATEL # 27

Malizia, A., et al., accepted for publication in ApJL

Markwardt, C. B., Smith, E., & Swank, J. H. 2003, IAU Circ. 8080

Markwardt C. B & Swank J. H., ATEL # 156

Markwardt C. B & Swank J. H., ATEL 133

Masetti, N., Palazzi, E., Bassani, L., et al. 2004, A&A, 426, 41

Masetti, N., Dal Fiume, D., Amati, L., et al. 2004, A&A, 423, 311

Masetti, N., Bassani, L., Bird, A.J. et al. 2005, ATEL # 528.

Mirabel, I. F., Rodriguez, L. F., Cordier, B., et al. 1992, Nature, 358, 215

Mirabel I. F. & Rodriguez L. F. 1994, Nature, 371,46

Molina, M., Bassani, L., Malizia, A., et al. 2004, ATEL # 263

Monet, D. G., Levine, S. E., Canzian, B., et al. 2003, AJ, 125, 984

Motch, C., Guillout, P., Haberl, F., et al. 1998, A&AS 132, 341

Negueruela, I., Marco, A., Speziali, R., et al. 2000, IAU Circ. 7541

Orosz, J. A., Groot, P. J., van der Klis, M., et al. 2002, Ap.J, 568, 845

Patel, S. K., Kouveliotou, C., Tennant, A., et al. 2004, ApJ, 602, 245

Raguzova, N. V., Popov, S. B. 2005, astro-ph/05505275

Remillard R.A. 1999, MemSAI, 70, 881

Remillard, R. A., Smith, D. A., Hurley, K. 2002, IAU Circ. 7880

Revnivtsev, M. 2003, Astron. Lett. 29, 644

Revnivtsev, M., Churazov, E. M., Sazonov, S. Yu., et al. 2004, A&A, 425, 49

Reynolds, A.P. , Parmar, A.N., Hakala, P.G., et al. 1999 A&AS, 134, 287

Rodriguez, J., Cabanac, C., Hannikainen, D. C., et al. 2005, A&A, 432, 253

Rodriguez, J., Tomsick, J. A., Foschini, L., et al. 2003, A&A, 407, 41

Rodriguez, L. F., Mirabel, I. F., Marti, J., et al. 1992, ApJ, 401, 15

Rupen, M. P., Brocksopp, C., Mioduszewski, A. J., et al. 2003, IAU Circ. 8054

Sekimoto, Y., Matsuzaki, K., Kamae, T., et al. 2000, PASJ, 52, 31

Sidoli, L., Vercellone, S., Mereghetti, S., et al. 2005, A&A, 429, 47

Stephen, J. B., Bassani, L., Molina, M., et al. 2005, A&A, 432, 49

Stephen, J. B., 2005, submitted to A&A

Sunyaev, R., Churazov, E., Gilfanov, M., et al. 1991, ApJ, 383, 49

Swank, J. & Morgan, E. 2000, IAU Circ. 7531

Torres, M.A.P., Garcia, M.R., McClintock, J.E., et al. 2004, ATEL # 264

Ubertini, P., Lebrun. F., Di Cocco, G., et al. 2003, A&A, 411, L131

Ubertini, P., et al. 2005, Adv. in Sp. Res., in press

Ubertini, P., et al. 2005, ApJ, 629, L109

Vasisht, G. & Gotthelf, E. V. 1997, ApJ, 486, 129

Veron-Cetty, M.-P., & Veron, P. 2003, A&A, 412, 399

Voges, W., Aschenbach, B., Boller, Th., et al. 1999, A&A 349, 389

Walter, R., Courvoisier, T. J.-L., Foschini, L., et al. 2004, ESA-SP 522, 417

Walter, R., & INTEGRAL Survey Team. 2004, AAS/High Energy Astrophysics Division 8

Walter, R., Rodriguez, J., Foschini, L., et al. 2003, A&A, 411, 427

Wamsteker, W., Prieto, A.,Vitores, A., et al. 1985, A&AS, 62, 255

Wen,L., Levine,A., Bradt, H. 1999, BAAS31, 1427

Winkler, C., et al. 2004, ESA SP-552, 7

Woods, P., Kouveliotou, C., Finger, M. H., et al. 2002, IAU Circ. 7856

Zacharias N., Urban S.E., Zacharias M.I., et al. 2000, AstJ, 120, 2131

in't Zand, J.J.M., Cornelisse, R., & Mendez, M. 2005, A&A, 440, 287

in't Zand, J.J.M., Jonker, P.G., Nelemans, G., et al. 2005 A&A submitted

in't Zand, J.J.M., Verbunt, F., Kuulkers, E., et al. 2002, A&A, 389, 43

Zimmermann, H.-U., Boller, Th., Dbereiner, S., Pietsch, W. 2001, A&A, 378, 30

Table 2. 2nd IBIS/ISGRI Catalog

Name	RA	Dec	Err($'$)	F_{20-40}	F_{40-100}	Signif	Exp	Type	Refs
V709 Cas	7.252	59.317	1.3	4.1±0.5	<2.9	6.9*	79	CV	1
RX J0053.8-7226	13.531	-72.426	1.2	3.3±0.4	<2.3	7.6*	106	HMXB, XP, T, Be	2 , 3
gam Cas	14.126	60.702	1.1	5.2±0.5	<2.9	8.8*	77	HMXB, Be	2 , 3
SMC X-1	19.324	-73.444	0.5	39.6±0.4	9.2±0.8	86.7*	106	HMXB, XP	2
1A 0114+650	19.511	65.288	0.7	10.3±0.5	5.3±1.0	17.5*	78	HMXB, XP	2
QSO B0241+62	41.184	62.510	1.4	3.7±0.7	5.8±1.2	6.4**	51	AGN,Sy1.2	4
X Per[a]	58.842	31.036	0.9	50.1±4.8	51.0±7.5	11.2**	2	HMXB, XP, Be	2 , 3
LMC X-4[b]	83.221	-66.365	0.6	50.3±1.5	12.0±2.5	33.5*	23	HMXB, XP	2
Crab	83.628	22.020	0.5	1000.0	1000.0	1691.0**	97	PWN, PSR	5
MCG+08-11-011	88.745	46.454	1.4	6.1±1.0	<5.5	6.2*	23	AGN, Sy1.5	4
4U 0614+091	94.270	9.145	0.6	24.7±0.8	22.8±1.4	29.5**	46	LMXB, B, A	6
IGR J07506-1547	117.647	-15.788	1.7	2.2±0.6	4.2±1.1	5.3**	64	?	
IGR J07565-4139	119.123	-41.642	1.3	1.0±0.2	<0.8	6.8*	949	?	
IGR J07597-3842	119.930	-38.730	0.9	2.3±0.2	1.9±0.3	11.4**	774	AGN?	7
ESO 209-12	120.483	-49.738	0.9	1.4±0.2	1.8±0.3	11.3**	939	AGN, Sy1.5	4
Vela Pulsar	128.816	-45.184	0.5	6.9±0.1	8.2±0.2	64.8**	1450	PWN, PSR	5
4U 0836-429	129.338	-42.893	0.5	36.6±0.1	31.1±0.2	240.9**	1400	LMXB, T, B	6
FRL 1146	129.633	-36.008	1.2	1.3±0.2	0.9±0.3	7.9*	881	AGN, Sy1	4
Vela X-1	135.512	-40.557	0.5	216.9±0.1	48.1±0.2	1440.1*	1220	HMXB, XP	2
IGR J09026-4812	135.638	-48.196	1.1	0.9±0.1	0.9±0.2	8.5*	1350	?	
4U0919-54	140.050	-55.187	0.7	3.6±0.2	2.6±0.4	16.1**	602	LMXB	6
EXMS B0918-549E[c] [d]	140.022	-55.143	0.9	-	-	12.0*	602	?,T	
MCG-05-23-016	146.869	-30.930	1.0	10.2±1.4	8.4±2.0	9.9**	27	AGN, Sy1i	4
GRO J1008-57[e]	152.396	-58.294	0.9	<1.3	<2.2	11.6	130	HMXB, XP, Be, T	2 , 3
IGR J10404-4625	160.095	-46.416	1.5	2.9±0.7	5.9±1.1	5.7**	102	AGN?	8
IGR J11114-6723	167.854	-67.392	1.7	1.7±0.4	2.3±0.7	5.1**	199	?	
Cen X-3	170.300	-60.638	0.5	27.4±0.4	3.6±0.6	71.9*	209	HMXB, XP	2
1E 1145.1-6141[f] [g]	176.866	-61.957	0.5	30.1±0.3	17.5±0.5	83.4**	269	HMXB, XP	2
2E 1145.5-6155[h]	177.016	-62.199	0.7	7.9±0.3	4.6±0.5	17.5*	274	HMXB, XP, Be, T	2 , 3
NGC 4151	182.640	39.401	0.5	32.7±0.6	40.0±1.0	42.4**	56	AGN, Sy1.5	4
4C 04.42	185.606	4.239	1.4	1.4±0.4	3.9±0.6	6.5**	213	AGN, QSO	4
NGC 4388	186.446	12.637	0.6	15.4±0.9	16.7±1.4	21.0**	62	AGN, Sy1h	4
GX 301-2	186.653	-62.776	0.5	112.8±0.3	14.4±0.4	401.1*	406	HMXB, XP, T	2
3C 273	187.293	2.027	0.6	7.5±0.3	8.5±0.5	28.2**	279	AGN, QSO	4
IGR J12349-6433	188.709	-64.570	0.7	4.5±0.3	2.8±0.4	16.8*	437	Symb	9
NGC 4507	188.912	-39.903	0.7	10.7±0.7	12.2±1.1	17.5**	63	AGN, Sy1h	4
LEDA 170194	189.796	-16.182	1.2	2.6±0.5	5.6±0.9	7.6**	111	AGN?	8
NGC 4593	189.927	-5.353	0.7	4.1±0.3	4.0±0.5	16.2**	349	AGN, Sy1	4
4U 1246-588	192.351	-59.091	1.1	2.0±0.3	2.0±0.4	8.3**	436	HMXB, T	2
3C 279	194.038	-5.781	1.2	1.9±0.3	2.2±0.5	7.5**	326	Blazar	4
1H 1254-690	194.361	-69.305	1.2	2.5±0.3	<1.4	7.7*	369	LMXB, B, D	6
Coma cluster	194.880	27.961	1.3	1.9±0.3	<1.5	7*	251	Cluster	5
IGR J13020-6359	195.541	-63.925	1.1	2.1±0.2	1.3±0.4	8.4*	501	?	
NGC 4945	196.362	-49.476	0.5	11.4±0.4	18.5±0.7	38.2**	226	AGN, Sy2	10
Cen A	201.364	-43.021	0.5	49.7±0.4	63.8±0.8	129.2**	112	AGN, Sy2	11
4U 1323-62	201.650	-62.126	0.7	3.8±0.2	2.4±0.4	16.9*	535	LMXB, B, D	6

Table 2—Continued

Name	RA	Dec	Err(′)	F_{20-40}	F_{40-100}	Signif	Exp	Type	Refs
4U 1344-60	206.872	-60.604	0.7	3.9±0.2	4.7±0.4	19.9**	526	AGN?	8
IC 4329A	207.348	-30.323	1.1	10.0±1.1	8.1±1.8	8.6**	29	AGN, Sy1.2	4
Circinus Galaxy	213.274	-65.343	0.5	14.0±0.2	11.5±0.4	62.3*	487	AGN, Sy1h	4
IGR J14492-5535	222.305	-55.579	1.5	1.5±0.2	<1.2	5.7*	520	?	
PSR B1509-58	228.466	-59.147	0.5	8.6±0.2	11.0±0.4	44.4**	509	PSR	12
Cir X-1[i]	230.178	-57.174	0.5	15.6±0.2	<1.2	59.6*	512	LMXB, T, B, A	6
IGR J15359-5750	233.965	-57.832	1.3	1.2±0.2	2.0±0.4	7.0**	505	?	
4U 1538-522	235.600	-52.378	0.5	22.6±0.2	3.0±0.4	91.9*	553	HMXB, XP	2
4U 1543-624	236.947	-62.577	0.9	2.9±0.3	<1.4	10.8*	386	LMXB	6
IGR J15479-4529	237.033	-45.484	0.6	5.4±0.2	2.4±0.4	20.9*	544	CV	13 , 14
XTE J1550-564	237.746	-56.482	0.5	115.1±0.2	176.5±0.4	628.1**	525	LMXB, T, BH	6 , 15
4U 1608-522	243.175	-52.434	0.5	14.8±0.2	11.9±0.3	68.4**	648	LMXB, T, B, A	6
IGR J16167-4957	244.139	-49.985	1.0	2.1±0.2	<1.0	9.3*	682	?	
IGR J16194-2810	244.858	-28.160	1.5	2.2±0.3	<1.5	6.0*	349	?	16
AX J161929-4945[j]	244.865	-49.727	0.9	2.2±0.2	1.9±0.3	10.5**	690	HMXB, NS?	17
Sco X-1	244.988	-15.648	0.5	716.9±0.6	16.3±0.9	1060.0*	110	LMXB, Z	6
IGR J16207-5129	245.195	-51.504	0.8	3.3±0.2	2.4±0.3	14.9**	676	?	
4U 1624-490	247.012	-49.204	0.7	4.2±0.2	<1.0	18.7*	715	LMXB, D	6
IGR J16318-4848	247.942	-48.824	0.5	29.3±0.2	14.4±0.3	129.1*	724	HMXB, T	18
AX J1631.9-4752	248.006	-47.870	0.5	17.1±0.2	6.6±0.3	78.3*	737	HMXB, T, XP	19 , 20
4U 1626-67	248.098	-67.456	0.6	16.1±0.5	<2.3	31.0*	181	LMXB, XP	6
4U 1630-47	248.517	-47.398	0.5	63.5±0.2	44.9±0.3	290.5**	742	LMXB, T, U, D, BHC	6
IGR J16358-4726	248.970	-47.421	0.7	4.3±0.2	2.4±0.3	19.7*	747	LMXB?, T	21
IGR J16377-6423[k]	249.420	-64.382	1.6	2.2±0.4	<1.8	5.6*	235	Cluster?	22 , 16
AX J163904-4642[l]	249.763	-46.693	0.6	6.9±0.2	<1.0	32.9*	760	HMXB?, T, XP	23 , 24 , 25
4U 1636-536	250.222	-53.755	0.5	24.2±0.2	13.4±0.4	106.5*	641	LMXB, B, A	6
IGR J16418-4532	250.440	-45.532	0.6	5.2±0.2	1.3±0.3	23.0*	784	?	
GX 340+0	251.447	-45.612	0.5	34.9±0.2	2.1±0.3	158.7*	794	LMXB, Z	6
IGR J16479-4514	252.004	-45.207	0.7	3.9±0.2	2.7±0.3	18.2*	805	HMXB?	26
IGR J16482-3036	252.040	-30.593	1.1	1.6±0.2	1.6±0.3	8.4**	857	AGN?	8 , 16
IGR J16493-4348[m]	252.381	-43.835	0.8	2.7±0.2	2.2±0.3	13.3**	847	XB?	27
IGR J16500-3307	252.505	-33.116	1.2	1.7±0.2	<0.9	7.8*	966	?	16
ESO 138-1[n]	252.938	-59.213	1.3	1.9±0.3	1.6±0.4	6.7**	402	AGN, Sy2	4
IGR J16558-5203	254.012	-52.052	1.0	1.4±0.2	2.5±0.4	9.1**	660	?	
AX J1700.2-4220	255.073	-42.396	1.2	1.4±0.2	1.3±0.3	7.6**	946	?	
OAO 1657-415	255.206	-41.661	0.5	85.1±0.2	45.8±0.3	402.6*	980	HMXB, XP	2
GX 339-4	255.708	-48.791	0.5	22.7±0.2	28.2±0.3	126.1**	710	LMXB, T, U, BH	6 , 28
4U 1700-377	255.988	-37.849	0.5	207.3±0.2	124.6±0.3	1110.2**	1180	HMXB	2
GX 349+2	256.448	-36.419	0.5	46.0±0.2	1.6±0.3	241.5*	1220	LMXB, Z	6
4U 1702-429	256.566	-43.055	0.5	14.9±0.2	9.3±0.3	71.1*	921	LMXB, B, A	6
IGR J17088-4008	257.208	-40.142	0.9	1.1±0.2	2.2±0.3	10.3**	1110	AXP	6
4U 1705-440	257.226	-44.107	0.5	27.3±0.2	16.4±0.3	124.4*	863	LMXB, B, A	6
4U 1705-32	257.237	-32.317	0.7	2.9±0.2	3.0±0.3	19.3**	1290	LMXB, B	29
IGR J17091-3624	257.278	-36.415	0.5	10.0±0.2	13.2±0.3	71.5**	1260	BHC?	30
XTE J1709-267[o]	257.389	-26.655	0.7	1.0±0.2	<0.8	18.4	1140	LMXB, B, T	6
XTE J1710-281	257.550	-28.140	0.6	3.0±0.2	4.1±0.3	22.0**	1210	LMXB, T, B	6

Table 2—Continued

Name	RA	Dec	Err(′)	F_{20-40}	F_{40-100}	Signif	Exp	Type	Refs
Oph Cluster[p]	258.109	-23.363	0.6	4.9±0.2	1.7±0.3	25.6*	1020	Cluster	31
4U 1708-40	258.139	-40.850	1.3	1.2±0.2	<0.8	6.9*	1060	LMXB, B	6
SAX J1712.6-3739	258.146	-37.655	0.6	5.2±0.2	4.5±0.3	31.0**	1250	LMXB, T, B	6
V2400 Oph	258.170	-24.267	0.7	3.5±0.2	2.1±0.3	19.4*	1070	CV	1
XTE J1716-389	258.941	-38.835	1.1	1.6±0.2	1.0±0.3	8.8*	1200	?	16
NGC 6300	259.213	-62.823	1.0	4.3±0.4	3.7±0.7	10.1**	200	AGN, Sy2	4
IGR J17195-4100	259.931	-41.032	0.8	2.3±0.2	2.2±0.3	13.9**	1060	?	
XTE J1720-318	259.976	-31.749	0.5	6.1±0.2	8.1±0.2	49.4**	1410	LMXB, T, BHC	32
IGR J17200-3116	260.022	-31.290	0.7	3.0±0.2	2.3±0.2	19.4**	1430	?,T	
IGR J17204-3554[q]	260.104	-35.900	0.8	1.5±0.2	2.1±0.2	13.1**	1360	mol cloud?	33
EXO 1722-363[r]	261.288	-36.277	0.5	8.9±0.2	3.2±0.2	51.8*	1360	HMXB, XP	2
IGR J17254-3257	261.350	-32.968	0.7	2.7±0.2	3.0±0.2	19.9**	1450	?	
GRS 1724-30	261.884	-30.812	0.5	18.2±0.2	16.0±0.2	125.6**	1470	LMXB, G, B, A	6
IGR J17285-2922	262.172	-29.382	1.2	0.7±0.2	1.4±0.2	7.3**	1470	BHC?, T	34
IGR J17303-0601	262.593	-6.016	0.9	3.7±0.3	2.1±0.5	11.6*	282	LMXB?,CV?	35 , 36
GX 9+9	262.927	-16.974	0.5	12.9±0.2	1.6±0.3	53.8*	722	LMXB, A	6
GX 354-0	262.988	-33.830	0.5	44.1±0.2	16.8±0.2	264.1*	1460	LMXB, B, A	6
GX 1+4	263.004	-24.752	0.5	42.5±0.2	31.0±0.2	259.2**	1330	LMXB, XP	6
4U 1730-335	263.354	-33.390	0.8	2.4±0.2	<0.7	15.0*	1470	LMXB, G, RB, T	6
GRS 1734-294	264.381	-29.136	0.6	5.4±0.1	3.9±0.2	33.5**	1510	AGN, Sy1	4
SLX 1735-269	264.567	-26.995	0.5	9.3±0.2	7.5±0.2	61.6**	1460	LMXB, B	6
4U 1735-444	264.744	-44.451	0.5	29.6±0.2	1.3±0.3	132.3*	767	LMXB, B, A	6
XTE J17391-3021	264.818	-30.347	1.1	1.3±0.1	0.9±0.2	8.5**	1510	HMXB, NS, Be?, T	2 , 37 , 3
XTE J1739-285[s]	264.961	-28.496	1.1	<0.4	<0.7	8.4	1500	LMXB?	38
SLX 1737-282	265.191	-28.280	0.6	3.2±0.1	3.3±0.2	23.8**	1490	LMXB, B	6 , 39
2E 1739.1-1210	265.463	-12.196	1.1	2.2±0.2	1.8±0.4	8.8**	526	AGN, Sy1	40
XTE J1743-363	265.751	-36.381	0.8	2.5±0.2	1.9±0.2	14.6**	1340	?,T	
1E 1740.7-2942[t]	265.988	-29.745	0.5	26.7±0.1	34.0±0.2	222.0**	1510	LMXB, BHC	6 , 41 , 42
IGR J17445-2747	266.132	-27.783	1.5	0.9±0.1	0.8±0.2	6.0*	1480	?	
KS 1741-293[u]	266.220	-29.340	0.5	8.8±0.1	7.8±0.2	62.3**	1510	LMXB, T, B	6
IGR J17456-2901[v w]	266.410	-29.020	0.6	5.0±0.1	2.7±0.2	30.9*	1500	?	43
1E 1742.8-2853[w]	266.498	-28.917	0.6	5.4±0.1	3.7±0.2	31.8*	1500	LMXB	6
1A 1742-294	266.520	-29.510	0.5	14.1±0.1	7.9±0.2	85.7*	1510	LMXB, B	6
IGR J17464-3213	266.567	-32.232	0.5	66.5±0.2	40.5±0.2	405.1*	1490	LMXB, T, BHC	6 , 44
1E 1742.9-2849[w]	266.570	-28.814	0.6	5.4±0.1	2.8±0.2	31.6*	1500	LMXB	6
1E 1743.1-2843[w]	266.590	-28.670	0.8	3.8±0.1	1.6±0.2	13.5*	1500	LMXB	6
SAX J1747.0-2853[x]	266.805	-28.837	1.1	1.4±0.1	<0.7	8.8*	1500	LMXB, B, T	6
IGR J17475-2822	266.820	-28.445	0.7	2.1±0.1	1.9±0.2	15.1**	1490	mol cloud?	45
SLX 1744-299	266.860	-30.020	0.5	8.8±0.1	5.7±0.2	56.5*	1500	LMXB, B	6
GX 3+1	266.989	-26.562	0.5	13.5±0.2	0.8±0.2	84.7*	1440	LMXB, B, A	6
1A 1744-361	267.057	-36.133	1.2	1.0±0.2	1.3±0.2	7.7**	1340	LMXB, T	6
IGR J17488-3253	267.206	-32.914	0.7	2.3±0.2	3.3±0.2	19.4**	1460	?	
4U 1745-203	267.217	-20.386	0.7	2.1±0.2	3.2±0.3	16.1**	1070	LMXB, T, G	6
4U 1746-370	267.557	-37.047	0.6	4.7±0.2	1.9±0.3	25.5*	1270	LMXB, G, B, A	6
GRS 1747-312	267.637	-31.296	1.1	1.1±0.2	1.1±0.2	8.4**	1480	LMXB, G, T	6
IGR J17513-2011	267.822	-20.188	0.8	2.0±0.2	2.5±0.3	13.4**	1060	?	16

Table 2—Continued

Name	RA	Dec	Err(′)	F_{20-40}	F_{40-100}	Signif	Exp	Type	Refs
IGR J17544-2619	268.605	-26.342	1.3	1.1±0.2	<0.7	6.7*	1410	HMXB?, T	46 , 47 , 16
IGR J17597-2201	269.939	-22.033	0.5	8.4±0.2	7.8±0.3	52.2**	1190	LMXB, B, D	48 , 37
GX 5-1	270.287	-25.079	0.5	55.3±0.2	3.2±0.2	318.9*	1340	LMXB, Z	6
GRS 1758-258	270.303	-25.749	0.5	39.5±0.2	48.1±0.2	291.9**	1350	LMXB, U, BHC	6 , 49
GX 9+1	270.388	-20.524	0.5	17.6±0.2	0.9±0.3	93.0*	1080	LMXB, A	6
IGR J18027-1455	270.690	-14.922	0.7	3.0±0.2	3.3±0.3	15.5**	766	AGN, Sy1	35
SAX J1802.7-201[y]	270.692	-20.294	0.6	5.8±0.2	2.5±0.3	30.5*	1070	HMXB, T, XP	50 , 51
IGR J18048-1455	271.211	-14.914	1.0	1.7±0.2	2.0±0.3	9.3**	774	?	
XTE J1807-294	271.748	-29.410	0.6	3.1±0.2	3.1±0.2	21.6**	1340	LMXB, T, XP	52
SGR 1806-20	272.156	-20.423	0.6	3.4±0.2	4.7±0.3	23.7**	1060	SGR	53
IGR J18135-1751[y]	273.363	-17.849	1.1	1.6±0.2	1.2±0.3	8.2**	916	?	54
GX 13+1	273.618	-17.146	0.5	17.5±0.2	5.0±0.3	84.5*	880	LMXB, B, A	6
M 1812-12	273.779	-12.102	0.5	25.7±0.2	25.5±0.3	137.7**	735	LMXB, B	6
GX 17+2	274.007	-14.040	0.5	58.4±0.2	3.2±0.3	263.9*	781	LMXB, B, Z	6
SAX J1818.6-1703	274.671	-17.055	1.4	1.2±0.2	1.2±0.3	6.5**	869	?,T	
IGR J18193-2542	274.820	-25.703	1.5	0.8±0.2	1.1±0.3	5.7**	1130	?	
AX J1820.5-1434	275.133	-14.572	0.6	5.1±0.2	3.3±0.3	23.4*	794	HMXB, XP, Be	2 , 3
IGR J18214-1318	275.340	-13.308	0.9	2.1±0.2	2.0±0.3	10.8**	773	?	
4U 1820-303	275.928	-30.370	0.5	35.3±0.2	2.3±0.3	186.6*	1070	LMXB, G, B, A	6
4U 1822-000	276.335	-0.032	1.0	2.4±0.2	<1.1	9.9*	641	LMXB	6
IGR J18256-1035	276.406	-10.587	1.5	1.2±0.2	<1.0	5.9*	762	?	
3A 1822-371	276.462	-37.102	0.5	34.1±0.2	4.3±0.3	162.5*	895	LMXB, D	6
IGR J18259-0706	276.485	-7.106	1.4	1.2±0.2	1.0±0.3	6.2**	743	?	
GS 1826-24	277.367	-23.801	0.5	73.3±0.2	58.6±0.3	359.8**	942	LMXB, B	6
IGR J18325-0756	278.118	-7.940	0.7	3.9±0.2	2.2±0.3	18.2*	794	?	
SNR 021.5-00.9	278.395	-10.558	0.7	2.8±0.2	3.3±0.3	15.9**	785	SNR, PWN	55
PKS 1830-211	278.405	-21.052	0.7	3.0±0.2	3.7±0.3	17.7**	843	AGN, QSO	4
RX J1832-330	278.921	-32.989	0.5	11.6±0.2	9.9±0.3	58.6**	823	LMXB, G, B, T	6
AX J1838.0-0655[z]	279.507	-6.904	0.8	2.1±0.2	3.1±0.3	14.1**	835	?	56
ESO 103-35	279.578	-65.431	1.4	5.9±0.9	4.5±1.5	6.2**	42	AGN, Sy1.9	4
Ser X-1	279.992	5.031	0.5	10.1±0.2	<0.9	48.7*	861	LMXB, B	6
AX J1841.0-0535	280.237	-5.602	1.5	1.0±0.2	1.1±0.3	6.0**	861	HMXB, XP, Be?	57
Kes 73	280.338	-4.949	0.7	2.0±0.2	3.8±0.3	15.1**	875	SNR, AXP	58
IGR J18450-0435	281.243	-4.602	1.8	1.0±0.2	<0.9	5.0**	907	?	
GS 1843+009	281.418	0.875	0.6	4.3±0.2	3.2±0.3	22.9**	970	HMXB, XP, Be, T	2 , 3
AX J1846.4-0258	281.622	-2.973	0.8	1.9±0.2	2.5±0.3	12.5**	940	SNR, PWN, AXP	59
IGR J18483-0311	282.064	-3.169	0.7	4.1±0.2	2.7±0.3	20.3*	945	?	
3A 1845-024	282.082	-2.424	1.3	1.3±0.2	0.9±0.3	6.7*	956	HMXB, XP, Be?, T	2 , 3
IGR J18490-0000	282.267	-0.025	1.4	1.2±0.2	0.9±0.3	6.4**	998	?	
4U 1850-087	283.266	-8.706	0.6	4.6±0.2	3.8±0.3	23.2**	804	LMXB, G, B	6
IGR J18539+0727	283.477	7.458	0.9	1.9±0.2	1.6±0.3	11.3**	1000	BHC?	30
V1223 Sgr[A]	283.755	-31.145	0.6	7.8±0.2	3.5±0.4	30.3*	512	CV	1
XTE J1855-026	283.877	-2.604	0.5	11.8±0.2	6.9±0.3	64.8*	969	HMXB, XP, T	2
2E 1853.7+1534	284.008	15.621	0.9	2.8±0.2	2.0±0.4	12.0**	578	AGN?	8
XTE J1858+034[B]	284.686	3.431	0.5	0.8±0.2	<0.8	49.8	1090	HXMB, XP, Be?, T	2 , 3
XTE J1901+014	285.397	1.439	0.6	3.4±0.2	3.0±0.3	21.6**	1070	T, BHC?	60

Table 2—Continued

Name	RA	Dec	Err(′)	F_{20-40}	F_{40-100}	Signif	Exp	Type	Refs
4U 1901+03	285.913	3.205	0.5	93.8±0.2	10.5±0.3	552.3*	1090	HMXB, T, XP	2 , 61
XTE J1908+094	287.220	9.390	0.6	3.6±0.2	4.2±0.3	23.7**	998	LMXB, T, BHC	62
4U 1907+097	287.414	9.836	0.5	16.5±0.2	2.0±0.3	91.4*	980	HMXB, XP, T	2
4U 1909+07	287.701	7.602	0.5	14.4±0.2	8.7±0.3	81.6*	1060	HMXB, XP	63
Aql X-1	287.811	0.577	0.5	9.4±0.2	5.1±0.3	53.8*	1010	LMXB, B, A, T	6
SS 433	287.957	4.974	0.5	14.5±0.2	7.3±0.3	89.0*	1090	HMXB	2
IGR J19140+0951[C]	288.525	9.872	0.5	9.5±0.2	5.7±0.3	54.7*	981	HMXB?, NS?	64 , 65
GRS 1915+105	288.798	10.940	0.5	288.1±0.2	108.8±0.3	1591.0*	926	LMXB, T, BH	6 , 66
4U 1916-053	289.697	-5.243	0.5	9.3±0.2	3.9±0.3	42.1*	682	LMXB, B, D	6
IGR J19284+0107	292.098	1.119	1.3	1.2±0.2	<0.9	6.8*	857	?	
IGR J19308+0530	292.692	5.502	1.4	0.8±0.2	1.5±0.3	6.6***	949	?	
RX J1940.1-1025	295.066	-10.408	1.1	3.0±0.3	2.1±0.6	8.1*	267	CV	1
NGC 6814	295.644	-10.332	1.0	3.1±0.3	3.9±0.6	9.9**	248	AGN, Sy1.5	4
KS 1947+300	297.396	30.210	0.5	38.4±0.6	23.9±1.0	55.6*	93	HMXB, T, XP	2 , 67 , 68
Cyg X-1	299.592	35.194	0.5	812.9±0.6	944.3±1.0	1417.3**	100	HMXB, BH, U	2
Cyg A	299.878	40.755	1.1	5.4±0.6	6.0±1.0	8.8**	91	AGN, Sy1.9	4
EXO 2030+375	308.046	37.630	0.5	38.9±0.5	20.4±0.8	74.6*	147	HMXB, XP, Be, T	2 , 3
Cyg X-3	308.108	40.953	0.5	201.1±0.4	82.2±0.7	418.4*	151	HMXB	2
SAX J2103.5+4545	315.891	45.743	0.5	33.4±0.4	18.5±0.7	78.4*	166	HMXB, XP, Be, T	2 , 3
IGR J21247+5058	321.151	50.980	0.7	5.7±0.4	8.1±0.7	16.3**	143	AGN, Sy1?	35
IGR J21335+5105	323.375	51.092	1.2	2.9±0.4	<2.1	7.8**	143	CV	1
1H 2140+433	325.745	43.587	1.1	4.4±0.4	<2.2	8.8*	127	Dwarf nova, CV	1
Cyg X-2	326.168	38.318	0.5	26.7±0.5	<2.7	43.9*	96	LMXB, B, Z	6
4U 2206+543	331.974	54.514	0.6	12.8±0.5	9.2±0.8	24.6*	114	HMXB, NS, Be	2 , 69 , 3
Cas A	350.822	58.792	1.1	3.9±0.5	3.3±0.9	8.0**	95	SNR	5

[1]Names in bold face indicate new detections since first catalog

[2]Position errors are expressed as radius of 1σ error circle

[3]Fluxes are expressed in units of mCrab; appropriate conversion factors are: (20-40 keV) 10 mCrab = 7.57×10^{-11} erg cm^{-2} s^{-1} = 1.71×10^{-3} ph cm^{-2} s^{-1}; (40-100 keV) 10 mCrab = 9.42×10^{-11} erg cm^{-2} s^{-1} = 9.67×10^{-4} ph cm^{-1} s^{-1}

[4]Maximimum significance is quoted in either (*) 20–40 keV band, (**) 20–100 keV band, (***) 30–60 keV band, (no mark) significance in one revolution

[5]Exposure is the corrected on-source exposure in ksec

[6]Source type classifications: A=Atoll source (neutron star); AGN=Active galactic nuclei; AXP=Anomalous X-ray pulsar; B=Burster (neutron star); Be=B-type emission-line star; BH=Black hole (confirmed mass evaluation); BHC=Black hole candidate; Cluster=Cluster of galaxies; CV=Cataclysmic variable; D=Dipping source; G=Globular Cluster X-ray source; HMXB=High-mass X-ray binary; LMXB=Low-mass X-ray binary; Mol Cloud=Molecular cloud; NS=Neutron Star; PSR=Radio pulsar; PWN=Pulsar wind nebula; QSO = Quasar; SGR=Soft gamma-ray repeater; SNR=Supernova remnant; Sy=Seyfert galaxy; Symb=Symbiotic star; T=Transient source; U=Ultrasoft source; XB=Galactic X-ray binary; XP=X-ray pulsar; Z=Z-type source (neutron star)

[a]4U0352+30 in 1st IBIS/ISGRI catalog (Cat1)

[b]Values derived from staring observations during revolutions 50,154 and 203.

[c]Detected during revolution 139

[d]Cannot recover fluxes due to proximity to 4U0919-54

[e]Detected during revolution 203

[f]A1145.1-6141 in Cat1

[g]Position taken from 1E catalog, due to blending with 2E1145.5-6155

[h]Position taken from 1E catalog, due to blending with 2E1145.1-6141

[i]4U1516-569 in Cat1

[j]IGR J16195-4945 in Cat1

[k]Triangulum Australis

[l]IGR J16393-4643 in Cat 1

[m]PSR J1649-4349 in Cat1

[n]Equally well associated with NGC 6221, also Sy2

[o]Detected during revolution 171

[p]EXMS B1709-232 in Cat1

[q]Tentative association with NGC6334

[r]IGRJ17254-3616 in Cat1

[s]Detected during revolution 120

[t]1E1740.7-2943 in Cat1

[u]M1741-293 in Cat1

[v]Within 1.1′ of Sgr A*

[w]Fluxes unreliable due to blending in final mosaic, see Section 3.6

[x]Detected during revolution 175

[y]IGR J18027-2016 in Cat1

[z]HESS source (SNR/PWN?)

[A]4U1849-31 in Cat1

[B]Detected during revolution 189

[C]IGR J19140+098 in Cat1

References. — (1) - Downes et al. (2001) (2) - Liu et al. (2000) (3) - Raguzova & Popov (2005) (4) - Veron-Cetty & Veron (2003) (5) - Forman et al. (1978) (6) - Liu et al. (2001) (7) - Molina et al. (2004) (8) - Bassani et al. (2005) (9) - Masetti et al. (2005) (10) - Done et al. (1996) (11) - Dermer & Gehrels (1995) (12) - Laurent et al. (1994) (13) - Haberl et al. (2002) (14) - Stephen et al. (2005a) (15) - Orosz et al. (2002) (16) - Stephen et al. (2005b) (17) - Sidoli et al. (2005) (18) - Walter et al. (2003) (19) - Rodriguez et al. (2003) (20) - Lutovinov et al. (2005a) (21) - Patel et al. (2004) (22) - Ebeling et al. (2002) (23) - Combi et al. (2004) (24) - Malizia et al. (2004) (25) - Walter et al. (2004b) (26) - Walter et al. (2004a) (27) - Grebenev et al. (2005) (28) - Cowley et al. (1987) (29) - in't Zand et al. (2005a) (30) - Lutovinov & Revnivtsev (2003) (31) - Arnaud et al. (1987) (32) - Rupen et al. (2003) (33) - Sekimoto et al. (2000) (34) - Barlow et al. (2005) (35) - Masetti et al. (2004a) (36) - Gaensicke et al. (2005) (37) - Lutovinov et al. (2005b) (38) - Harmon et al. (2004) (39) - in't Zand et al. (2002) (40) - Torres et al. (2004) (41) - Sunyaev et al. (1991) (42) - Mirabel et al. (1992) (43) - Bélanger et al. (2004) (44) - Markwardt et al. (2003c) (45) - Revnivtsev et al. (2004) (46) - Gonzalez-Riestra et al. (2004) (47) - Revnivtsev (2003) (48) - Markwardt et al. (2003b) (49) - Rodriguez et al. (1992) (50) - Augello et al. (2003) (51) - Hill et al. (2005) (52) - Markwardt et al. (2003a) (53) - Atteia et al. (1987) (54) - Ubertini et al. (2005b) (55) - Davelaar et al. (1986) (56) - Malizia et al. (2005) (57) - Bamba et al. (2001) (58) - Vasisht & Gotthelf (1997) (59) - Gotthelf & Vasisht (1998) (60) - Remillard et al. (2002) (61) - Galloway et al. (2003) (62) - Woods et al. (2002) (63) - Levine et al. (2004) (64) - in't Zand et al. (2005b) (65) - Rodriguez et al. (2005) (66) - Mirabel & Rodriguez (1994) (67) - Swank & Morgan (2000) (68) - Negueruela et al. (2000) (69) - Masetti et al. (2004b)